Influence of doping concentrations of Hf on structural and electrical properties of $Hf_xZn_{1-x}O$ thin films

P. Sateesh[a,*], M. Saritha[b], N. Hemanthkumar[a], T. Satya[c], B. Hemachandrarao[d], K. Sriranjani[e], K. Sakkaravarthi[f], N. N. Phani[b], K. Gopinath[b], P. Sivakumar[a]
[a]*Department of Physics, St.Peter'S Engineering College, T.S. -500100, India*
[b]*Department of Chemistry, St.Peter'S Engineering College, T.S. -500100, India*
[c]*Department of H&BS, G.PullareddyEngineering College, Kurnool -518002, India*
[d]*Department of Physics, Mallareddy Engineering college, T.S-500100, India*
[e]*Department of Physics, Pace Institute of Technology Sciences A.P-523001, India*
[f]*Department of Mathematics, St.Peter'S Engineering College, T.S. -500100, India*

HfxZn1−xO thin films (x=0, 2.5,3, 7.5, 10 and 15mol %) were deposited on glass substrates using Sol-gel process. The influence of the Hf concentration on the structural, electrical, and optical properties of the films was studied. It is found that Hf ions can be effectively doped into ZnO and all films crystallize in the hexagonal wurtzite structure with a preferred c-axis orientation. The lattice constants of Hf_xZn_{1-xO} films increase with the Hf contents. The HfxZn1−xO thin films structures of high-Hf-content films remain after annealing at 600 °C for 20 min. The optical band gap increases with the Hf content, but it decreases with the annealing temperature. The reduction of bandgap partly results from grain growth, which is due to the quantum confinement effect of the small grains. Hf doping increases the resistivity of ZnO owing to the disorder of the material structure and the higher bandgap, which results in more carrier traps and less thermally excited carriers in the conduction bands. Two FTIR peaks centered at about 1432 and 1056 cm^{-1} coexist in the fluorescent spectra. With increasing the Hf contents, the intensity of fluorescent peaks enhances remarkably. The Minimum resistivity reached 6.1 * 10^{-2} Ω cm after annealing with 3% Hf content.

(Received April 2, 2023; Accepted July 28, 2023)

Keywords: Concentration, Electrical, Films, Band gap, orientation, Quantum confinement effect

1. Introduction

ZnO is a very popular material that has been used in the science community for decades. It has got many favourable features, such as being non-toxic and cheap, and having high chemical stability, carrier concentration, and thermal conductivity[1,2] ZnO has a direct wide band gap (3.37 ev),[3,4] so it could be used in many applications that electrical and optical devices such as capacitors, solar cells, transistors, etc.5–7 HfO_2 is a very important material these days because of its high energy barrier, thermodynamic stability, and dielectric constant[8,9] On the other hand, HfO_2 has thought of using SiO2 thanks to these advanced properties in many applications like flash disks, MIM capacitor, and Random Access Memory (RAM)[10–13] In recent years, doped ZnO with IV group elements have been thought to increase electrical stability[14] due to which HfO_2 is considered to be the best examples. The contribution of ZnO with HfO_2 is relatively new and promising. It enhances the electrical and optical properties of ZnO due to its high tenability [15] Hf-doped ZnO structures have been fabricated by different techniques. Examples of these techniques are chemical vapour deposition (CVD), physical vapour deposition (PVD), metal-organic chemical vapour deposition (MOCVD), plasma-enhanced chemical vapour deposition (PECVD), atomic layer depositions (ALD), pulsed laser deposition (PLD), atomic layer chemical vapour deposition (ALCVD), radio-frequency (RF)-magnetron sputtering, chemical bath

* Corresponding author: satheesh.poonam@gmail.com
https://doi.org/10.15251/JOR.2023.194.401

deposition (CBD), successive ionic layer adsorption and reaction (SILAR) and sol-gel[16–21] for thin film and solid state, hydrothermal, co-precipitation, sonication, wet-chemical and sol-gel[22–28] for bulk materials. The Sol- gel method is one of the most common methods used in the production of nano-sized ceramic samples as well as in the production of high-quality thin films.

In this method, especially at low temperatures, cost-effective, nanoscale, high-purity materials can be produced, and it is easy to control components for hybrid structures. Some studies have been reported on Hf-doped ZnO thin film structures with unique electrical properties, especially 0%–3%Hf doped. For example, it was observed that minimum resistivity value of 1.2 × 10−3Ω cm and transmission of higher than 80% for 0.5 at% Hf doped ZnO from (0, 1, 3, 5, 7, 10 at%) Hf-doped ZnO samples by pulsed laser deposition,29 it was revealed 3.3 at% Hf doped ZnO has lowest resistivity 6.7 × 10−4 Ω.cm and transmittance value of %77 from 0< × ⩽6.7 at% (0, 1, 3, 5, 7 at%) Hf-doped ZnO samples using atomic layer deposition,30 it was revealed that 3 at% Hf doped ZnO has minimum resistivity value of 6.3 × 10−2 Ω.cm and crystallize value of 65 nm from (0, 1, 3, 5, 7 at%)Hf-doped ZnO samples while the resistivity was 38 × 10−3 Ω.cm, transmission of higher than 60%–70% and crystallize value of 81 nm for un-doped ZnO by solgel technique,31 it was shown that 3 at% Hf doped ZnO has minimum resistivity value of 5.6 × 10−3 Ω.cm from (0, **1**, 3, 5, 7 at%) Hf doped ZnO samples while the resistivity of un-doped ZnO was 38 × 10−3 Ω.cm by sol-gel technique, 32 it was obtained that 1 at%Hf-doped ZnO has ultra-low resistivity value of 4.2 × 10−3 Ω.cm and they observed that strong green emission peak at room temperature using the sol-gel method.33 Apart from these studies of Hf-doped ZnO thin films, to our knowledge, few studies have been reported on the characterization of Hf-doped ZnO nanopowders or bulk ceramic samples. In these studies, it was investigated radiation detection for scintillation properties 34 and photo catalytic activity under sunlight illumination properties.27 However, there is no published article on the AC electrical properties and detailed impedance spectroscopy of the Hf-doped ZnO ceramic sample. Considering all previous Hf-doped ZnO studies, the minimum concentration of Hf for the minimum resistivity value was 0.5.29 In this paper, X= 0, 2.5,3, 7.5, 10, and 15mol %) at% Hf-doped ZnO (HZO) ceramic sample was chosen to investigate the effect of doping on impedance properties at different temperatures and frequencies. For this purpose, Al/ZnO/Al and Al/HZO/Al devices were fabricated [29-32].

2. Experiment

ZnO and X= 0, 2.5,3, 7.5, 10, and 15mol %) at% Hf doping concentration (x = 0–15%) were successfully synthesized on flexible polyimide (PI) substrates by the sol-gel spin coating method. Firstly, ZnO sol was obtained by dissolving zinc acetate dehydrate [Zn(CH3COO)2·2H2O] (Sigma Aldrich) in propanol [C2H5OH] (99.5% Merck), and the solution was mixed on the magnetic stirrer at 343 K for 30 min. Afterward, monoethanolamine (MEA, C2H7NO) as a stabilizer was added into the solution keeping the molar ratio of MEA to zinc acetate at 1.0. Secondly, for preparing HZO sol, the ZnO was prepared as Aldrich) was added to the prepared sol. The molar ratio of MEA to zinc acetate and hafnium III chloride [HfCl4] (Sigma Aldrich) was kept at 1.0 in the solution. Until obtaining transparent and homogenous sols, each solution was separately mixed in a 363 K magnetic stirrer for one hour. Finally, the transparent sols were deposited PI Substrates using 3000 rpm by using the spin coating Method sintered for an hour at 793 K in a muffle furnace and at an hour, and then the flexible fine HfZnO films were formed. Top and bottom aluminum electrodes on the obtained HfZnO films were thermally evaporated under a 10−5 mbar vacuum with a thermal evaporation system for electrical measurements. The diameter of the evaporated Al dots of ZnO and HZO samples was 1.6 × 10−3 m and 1.5 × 10−3 m. The thicknesses of the samples were 1.45 × 10−3 m and 1.5 × 10−3 m, respectively. The phase structures of the samples were identified by XRD (Rigaku-Miniflex II) with Cu-Kα radiation, and the nanostructures were characterized by FESEM (Hitachi-SU500). AC electrical characteristics were collected on the Key sight E4990A By using Probe Station Summit 11000B-M Finds the Hall Mobility [43-48].

3. Result and discussion

Lattice parameters a and c are calculated by using Eq. 1 for wurtzite hexagonal structure, where h, k, l are Miller indices, and d is the spacing of the crystal layers. Nano films Characterization:—X-ray diffraction is a nondestructive analysis method that enables the determination of the crystallographic properties of materials. XRD measurement was performed with a step size of 0.02 in the 2θ range from 20° to 80° with a diffractometer equipped with Cu Kα1 radiation (λ = 1.5406 Å). X-ray diffraction patterns of ZnO and HZO films are shown in Fig. 1. X-ray patterns of both samples had a ZnO wurtzite structure (JCPDS No. 36–1451). No difference or extra peaks were found in the XRD pattern of the HZO sample. It was observed that the intensity of the peaks decreased with the addition of Hf atoms to the ZnO structure. This case is due to the decrease in the crystallinity of the structure. A slight shift was observed in the XRD pattern towards lower values of 2θ for HZO. The values 2θ for a peak of (101) were 36.24° and 36.22° for ZnO and HZO, respectively. The ionic radius of Hf4+ (0.71 Å–0.83 Å) is similar to Zn2+ (0.74 Å). Therefore, Hf4+ can substitute Zn2+ effectively without leading to crystal distortion and changing the crystal structure of ZnO.33 Also, Hf could be separated into a non-crystalline region at the grain boundary. Thus, the doping of Hf atoms might cause crystal defects and/or the widening of large grain boundaries. It is known the source of microstrain is crystal imperfections, such as excess volume of grain boundaries, vacancies and vacancy clusters, and dislocations.35 Also, an increase in microstrain and dislocation density means a decrease in crystal quality.36 Moreover, the doping of Hf atoms donors may provide more free electrons, causing an increase in carrier concentration, while a significant amount of these free electrons may be scattered by the grain boundary effect, resulting in low electron mobility in the crystal structure.32,37 Structural parameters of ZnO and HZO nanofilms were obtained by X-ray diffraction method.

$$\frac{1}{d^2} = \frac{4}{3}\left(\frac{h^2 + k^2 + hk}{a^2}\right) = + \frac{l^2}{c^2} \tag{1}$$

The average crystal size of the samples was derived from the width of the sharpest diffractometric peak using the theoretical models. The obtained peak intensity, position angle, and full width at half maximum (FWHM) XRD pattern data were used in the Scherrer (SH) method Eq. 2, the Williamson Hall (W-H) method Eq. 3, and Halder Wagner (H-W) method Eq. 5. The larger crystallite size and smaller FWHM values indicate better crystallization of the particles.36

$$D_{sh} = \frac{k\lambda}{\beta_{hkl} \cos\theta} \tag{2}$$

where DSH is the crystal size according to the Scherrer method, k is the particle shape factor (0.90) which depends on the crystal shape and size distribution, β_{hkl} is the full width at half maximum (FWHM) of the most intensive and sharpest diffractometric peak, and θ is the diffraction angle of the peak.

$$\delta = \frac{1}{D_{sh}^2} \tag{3}$$

The dislocation density (δ), which is the number of defects in the sample, was estimated with the Scherrer method's Eq. 3

$$E_{sh} = \beta_{hkl} \div 4 \tan\theta \tag{4}$$

In Eq. 4, micro stress (εSH) was estimated with the Scherrer method, and in Eq. 5; DWH is the average crystallite size according to the W-H method.

$$\beta_{hkl}\cos\theta = k\lambda \div D_{wh} + 4E_{wh}\sin\theta \quad (5)$$

According to the W-H method, a graph of β θ hkl cos versus 4sinθ was plotted from Eq. 5 for ZnO and HZO nanofilms and shown in Fig. 2. Using Eq. 5, DWH, and εWH for ZnO and HZO nanofilms were estimated from the y-intercept and slope of the corresponding linear fit, respectively.

The fact that no remarkable difference in a and c lattice parameters was observed indicates that Hf ions may prefer to accumulate at the grain boundaries instead of replacing them with Zn atoms (Fig. 1).27 The wurtzite structure has a hexagonal unit cell with two lattice parameters a and c in the ratio of c/= / = a 8 3 1.633 (in an ideal wurtzite structure).38 It is seen that the c/a value found in our study (1.603 and 1.600) is quite close to this value. Estimated crystallite sizes are 31 nm and 24 nm according to Scherrer's method, and estimated average crystallite sizes are 42 nm and 34 nm according to the W–H method and 40 nm and 21 nm according to the H-W method for ZnO and HZO, respectively. The average crystallite sizes obtained using the W–H and H-W methods are bigger than Scherrer's equation. The difference is mainly because Scherrer's equation may not account for the lattice strain effect on the peak broadening.39 calculated dislocation densities are 10 × 10−4 nm−2 and 17 × 10−4 nm−2 for ZnO, respectively. Estimated micro-strains are 3.63 × 10−3 and 4.50 × 10−3 according to Scherrer's method, 0.86 × 10−3 and 1.14 × 10−3 according to the W–H method, and 3.57 × 10−3 and 45.2 × 10−3 according to H-W method for ZnO and HZO, respectively. While the crystallite sizes in all models decrease under the doping effect, the dislocation density and micro-strain increase. While no significant difference was observed in the XRD patterns with Hf doping, the calculated crystallization parameters show a slight decrease in crystal quality.

The surface morphology and nanostructure of ZnO and HZO nanofilms samples were investigated with FESEM images obtained from the scanned area of both samples (Fig. 4). It was observed that with the Hf doping, the sample surface became smoother, and the crystal grains were smaller than ZnO. The particle sizes were determined to vary from about 30 nm to 150 nm for ZnO and from about 10 nm to 70 nm for HZO. As mentioned in the XRD results, the radii of Zn+ (0.71 Å–0.83 Å) and Hf+ (0.74 Å) atoms are similar. After doping Hf to the ZnO structure, some of the Hf atoms may replace the Zn ions. However, the Hf ionic radius can be larger than ZnO. In this case, Hf impurities occupy interstitial sites rather than substitution sites, and some Hf atoms are located at grain boundaries. When some of the Hf atoms may occupy the interstitial spaces instead of the displacement sites, Hf atoms at grain boundaries may be compressed ZnO grains, causing ZnO grains to shrink.29, 30 Therefore, Hf doping suppresses ZnO crystal growth, resulting in increased surface smoothness.30 and 31 The FESEM results are consistent with the crystal size change in the XRD results.

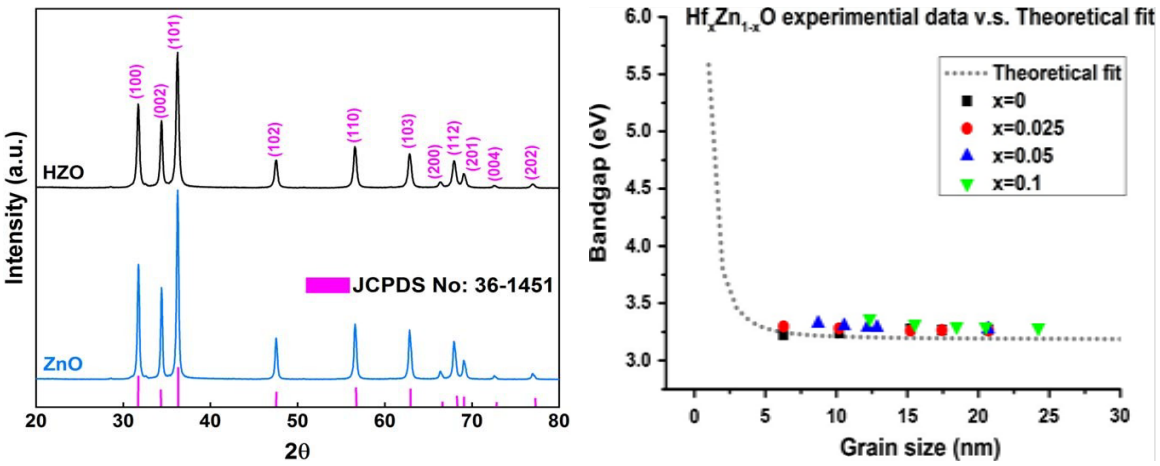

Fig. 1. XRD Patterns of ZnO and HZO films.

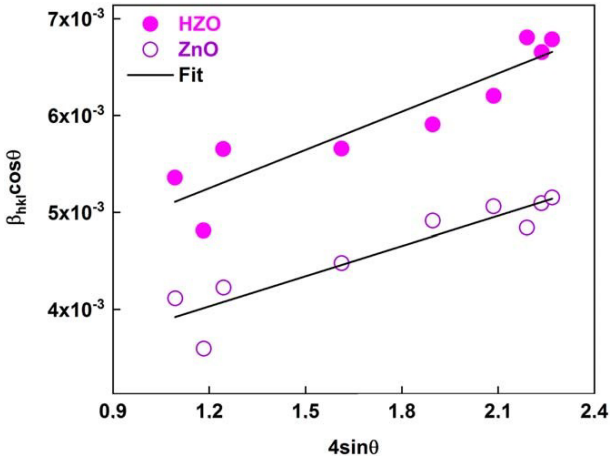

Fig. 2. According to W-H Method $\beta_{hkl} Cos\theta$ *VS 4Sinθ.*

Table 1. Lattice parameters of ZnO HZnO films.

Lattice Parameters			Crystal size			Dislocation Density $\delta \times 10^{-4}\ nm^{-2}$	Microstress $\times 10^{-3}$		
a (nm)	C (nm)	C/a	D_{sh}	D_{wH}	D_{HW}		ε_{sh}	ε_{WH}	ε_{hw}
0.325	0.522	1.601	32	41	40	11	3.62	0.88	3.57
0.324	0.521	1.589	26	34	22	17	4.50	1.12	45.4

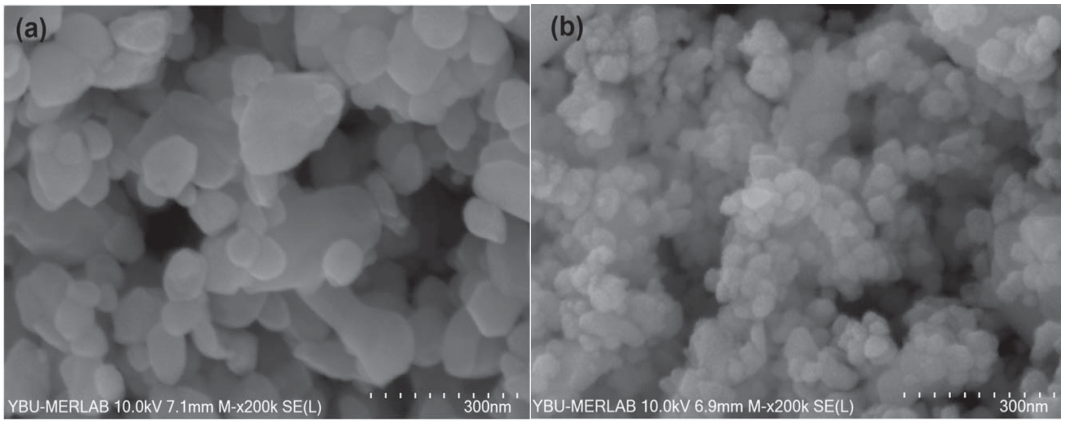

Fig. 3. FESEM Images of $HFZn_{1-x}O$ films.

The FESEM Images of the films deposited on glass substrates were measured to further Characterize The effect of Hf doping concentration on the Surface morphology of HfZno films. The band gap increased with the Hf content but decreased after thermal annealing

3.1. Electrical properties

3.1.1. Capacitance and conductance characterization

As a function of frequency, information about interface states can be given from both capacitance and conductivity measurements. The capacitance–frequency(C–f) plots of $HfZn_{1-x}o$ samples were obtained in the 25Hz–1.5MHz frequency and temperature range Fig 4 represents C − log f curves in different temperatures for ZnO and HZO devices.

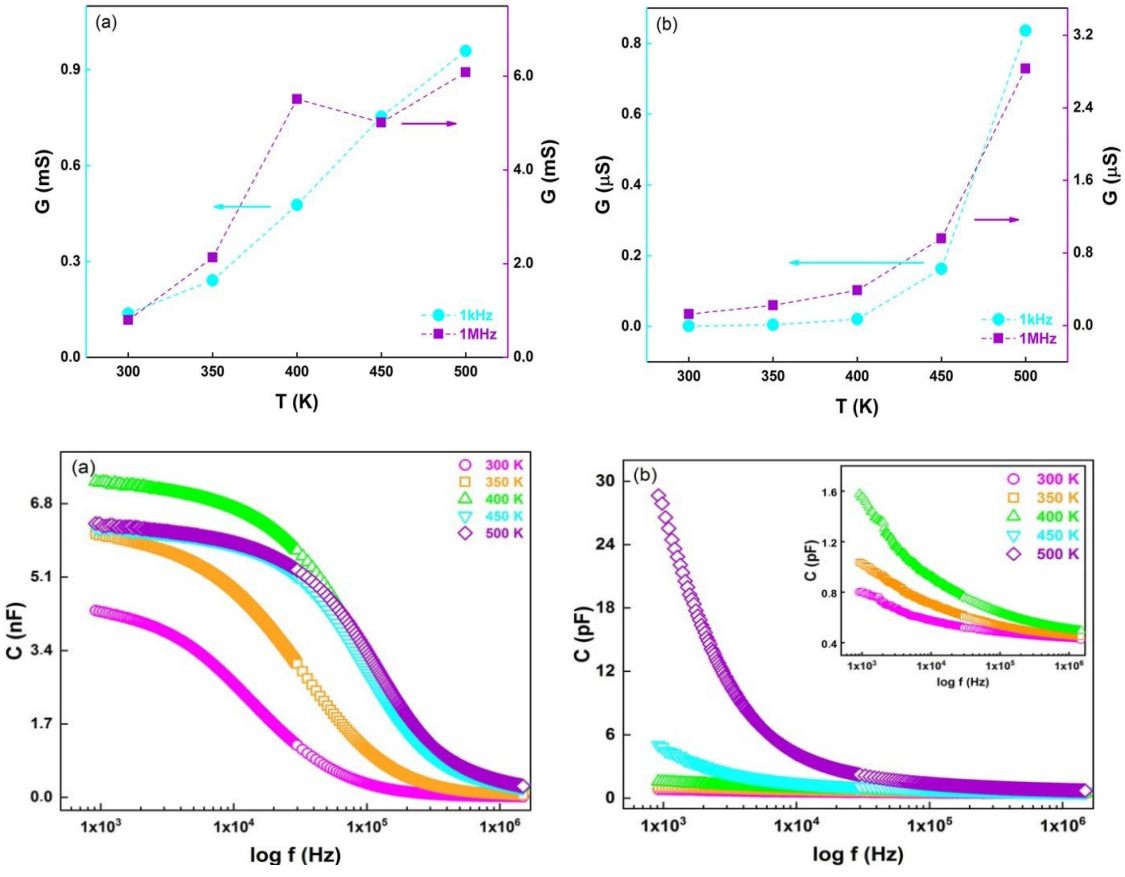

Fig. 4. Plots of C-logf & T-G (a) ZnO films (b) $HfZn_{1-x}O$ films.

Fig. 5a for ZnO, there is a slight decrease in the low-frequency region of the capacitance and a significant reduction up to the high frequency. C values of ZnO for 1 kHz at 300 K and 500 K are 4.29 and 6.28 nF, respectively. C values of ZnO for 1 MHz at 300 K and 500 K are 0.02 and 0.32 nF, respectively. In Fig. 5b. HZO, there is a maximum value in the low-frequency region of the capacitance, a decrease in the mid-frequency region, and saturation in the high-frequency region at all temperature values. C values HZO for 1 kHz at 300 K and 500 K are 0.72 and 26 pF, respectively. C values of HZO for 1 MHz at 300 K and 500 K are 0.4 and 0.8 pF, respectively. Charge carriers, which can follow the AC signal at the sample interface at low frequencies, caused high capacitance values at low frequencies. In addition, the increase in capacitance with increasing temperature at low-frequency regions in Fig. 5a is generally attributed to surface states or deep levels, 40, 41 while the decrease of capacitance with increasing temperature is attributed to the formation of interfacial space charge formation and temperature-dependent series resistance effect.42, 43

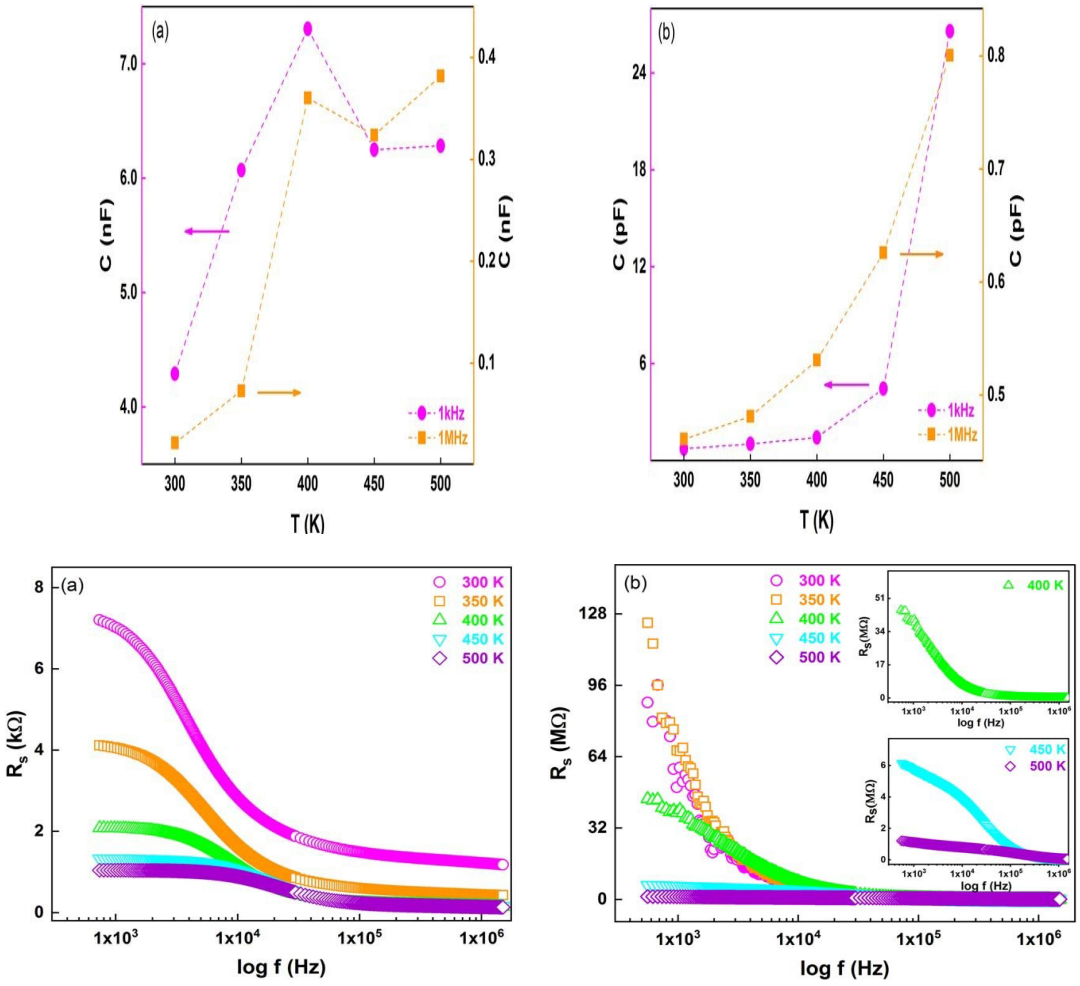

Fig. 5. Plots of C-T& logf-R (a) ZnO ilms (b) $HfZn_{1-x}O$ films Hall measurement.

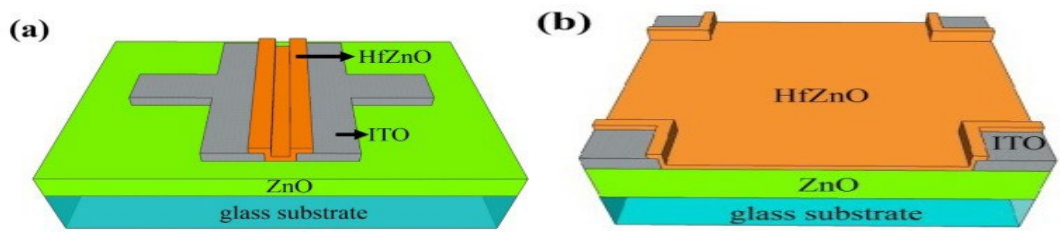

Fig. 6. The samples for (a) sheet resistance measurement, and (b) Hall measurement.

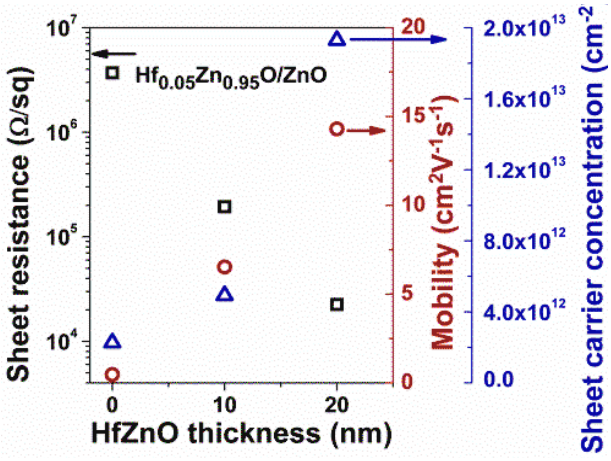

Fig. 7. Hall measurement results of the $Hf_{0.05}Zn_{0.95}O$/ZnO.

Figure 7 shows the Hall measurement results of the $Hf_xZn_{1x}O$/ZnO heterostructures increases of carrier concentration and carrier mobility are observed after depositing $Hf_xZn_{1x}O$ onto ZnO. For example, the sheet carrier concentration increased from 2.26×10^{12} cm^{-2} (bare ZnO) to 1.91×10^{13} cm^{-2} after depositing an 18-nm thick $Hf_{0.05}Zn_{0.95}O$. In a polycrystalline material system, the grain boundary potential strongly influences carrier transport. The induced carriers were confined at the interface to provide a stronger screening effect on the grain boundary [33-42], which there by reduced the grain boundary potential to improve the carrier mobility of the hetero structures. The carrier mobility increased from 0.45 $cm^2V^{-1}s^{-1}$ (bare ZnO) to 1 4.2 $cm^2V^{-1}s^{-1}$ after the deposition of a 18-nm- thick $Hf_{0.05}Zn_{0.95}O$.

4. Conclusions

In summary, HZO and ZnO bulk nanostructure were synthesized by sol-gel method. Surface morphologies and electrical properties of HZO and ZnO were compared. In both samples, the XRD pattern exhibited sharp and intense peaks, the hexagonal wurtzite structure of ZnO. Estimated crystallite sizes are determined as 31nm and 24nm according to Scherrer's method and estimated average crystallite sizes are founded 42 nm and 34 nm according to the W–H method, and 40nm and 21nm according to the H-W method for ZnO and HZO, respectively. Calculated dislocation densities are 10×10^{-4} nm^{-2} and 17×10^{-4} nm^{-2} for ZnO and HZO while micro-strains are 0.89×10^{-3} and 1.13×10^{-3}, respectively. Hf doping on the ZnO structure. FESEM images also showed that the particle size was reduced by Hf doping to the ZnO structure.

Capacitance, conductance, and impedance properties of ZnO and HZO nano structures brought into bulk form were investigated in 50 K steps in the frequency range of 25Hz–1.5MHz, the temperature range of 300K–500K. *C* and *G* values decrease when doping Hf to ZnO. Therefore, the R_s values increase with Hf doping. Hf doping can enhance the crystallinity of ZnO significantly. The ultraviolet emission band of HZO exhibits a blue shift. The intensity of the ultraviolet emission band rises with Hf-doping density. The resistivity of HZO film is 6.2×10^{-3} Ω cm, which is lower than AlZnO film.

Acknowledgments

The basic research was supported by JNTUH. The SEM, XRD and EDX, Hall measurement system analysis of samples is facilitated by OU and HCU Universities

References

[1] F. Ahmad and A. Maqsood, Mater. Sci. Eng. B Solid-State Mater. Adv. Technol., 273, 115431 (2021); https://doi.org/10.1016/j.mseb.2021.115431

[2] A. Toghan, A. Modwi, M. Khairy, and K. K. Taha, Chem. Phys., 551, 111350 (2021); https://doi.org/10.1016/j.chemphys.2021.111350

[3] K. Kandpal, N. Gupta, J. Singh, and C. Shekhar, J. Electron. Mater., 49, 3156 (2020); https://doi.org/10.1007/s11664-020-08055-4

[4] A. Wibowo, M. A. Marsudi, M. I. Amal, M. B. Ananda, R. Stephanie, H. Ardy, and L. J. Diguna, RSC Adv., 10, 42838 (2020); https://doi.org/10.1039/D0RA07689A

[5] B. Alfakes, J. Villegas, H. Apostoleris, R. Devarapalli, S. Tamalampudi, J. Lu, J. Viegas, I. Almansouri, and M. Chiesa, J. Phys. Chem. C, 123, 15258 (2019); https://doi.org/10.1021/acs.jpcc.9b02253

[6] M. Çavaş, J. Theor. Appl. Phys., 11, 325 (2017); https://doi.org/10.1007/s40094-018-0274-3

[7] N. Bouazizi, F. Ajala, M. Khelil, H. Lachheb, K. Khirouni, A. Houas, and A. Azzouz, J. Mater. Sci., Mater. Electron., 27, 11168 (2016); https://doi.org/10.1007/s10854-016-5235-5

[8] N. Tugluoglu, S. Karadeniz, and B. Bariş, Mater. Sci. Semicond. Process., 33, 199 (2015); https://doi.org/10.1016/j.mssp.2015.01.031

[9].K. S. Hemalatha, G. Sriprakash, M. V. N. Ambika Prasad, R. Damle, and K. Rukmani, J. Appl. Phys., 118, 154103 (2015); https://doi.org/10.1063/1.4933286

[10] J.-S. Bae, Y.-E. Jeong, S. Park, Applied Surface Science 321 (2014) 98; https://doi.org/10.1016/j.apsusc.2014.09.194

[11]M. Xi, X. Wang, Y. Zhao, Z. Zhu, H. Fong, Applied Physics Letters 104/13 (2014) 133102; https://doi.org/10.1063/1.4870296

[12] T.-P. Chen, K.-H. Lee, S.-P. Chang, S.-J. Chang, P.-C. Chang, Applied Physics Letters 103/2 (2013) 022101; https://doi.org/10.1063/1.4813107

[13]Sun, W. Yang, Y. Huang, W.S. Lai, A.Y. Lee, C.F. Wang, H. Gong, Journal of Applied Physics 112/8 (2012) 083709; https://doi.org/10.1063/1.4758383

[14]C.H. Ahn, J.H. Kim, H.K. Cho, Journal of the Electrochemical Society 159/4 (2012) H384; https://doi.org/10.1149/2.026204jes

[15]S. K. Mandal, T. K. Nath, and I. Manna, Nanosci. Nanotechnol. Lett., 1, 99 (2011); https://doi.org/10.1166/nnl.2009.1021

[16]. A. Tabib, N. Sdiri, H. Elhouichet, and M. Férid, J. Alloys Compd., 622, 687 (2015); https://doi.org/10.1016/j.jallcom.2014.10.092

[17]. M. Kumar, H. Jeong, and D. Lee, J. Alloys Compd., 720, 230 (2017); https://doi.org/10.1016/j.jallcom.2017.05.266

[18]. D. Singh, R. Gupta, and K. K. Bamzai, J. Mater. Sci., Mater. Electron., 28, 5295 (2017); https://doi.org/10.1007/s10854-016-6187-5

[19]. A. G. Hunt, Ac hopping conduction: Perspective from percolation theory, 81:9, 875 (2001); https://doi.org/10.1080/13642810108205779

[20]. B. P. Das, P. K. Mahapatra, and R. N. P. Choudhary, J. Mater. Sci., Mater. Electron., 15, 107 (2004); https://doi.org/10.1023/B:JMSE.0000005386.88365.19

[21]. E. G. El-Metwally, N. A. Hegab, and M. Mostfa, J. Mater. Sci., Mater. Electron., 33, 12384 (2022); https://doi.org/10.1007/s10854-022-08196-8

[22]. A. Radoń, D. Łukowiec, M. Kremzer, J. Mikuła, and P. Włodarczyk, Materials (Basel)., 11(5), 735 (2018); https://doi.org/10.3390/ma11050735

[23]. Z. Imran, M. A. Rafiq, and M. M. Hasan, AIP Adv., 4 (2014); https://doi.org/10.1063/1.4885462

[24]. A. Rahal, S. M. Borchani, K. Guidara, and M. Megdiche, R. Soc. Open Sci., 5 (2018).

[25]. M. H. Ghozza, I. S. Yahia, and S. I. El-Dek, Mater. Res. Express, 7, 056104 (2020); https://doi.org/10.1088/2053-1591/ab8ee2

[26]. A. A. Ebnalwaled, G. A. Gamal, H. A. Elshaikh, and M. M. Mahasen, 5, 1 (2016).
[27]. M. Pollak and B. I. Shklovskii, Hopping Transport in Solids, 28, 207 (1991); https://doi.org/10.1016/B978-0-444-88037-6.50013-0
[28]. H. I. Elsaeedy, A. Qasem, M. Mahmoud, H. A. Yakout, and S. A. Abdelaal, Opt. Mater. (Amst)., 111, 110693 (2021); https://doi.org/10.1016/j.optmat.2020.110693
[29]M.-C. Lin, Y.-J. Chang, M.-J. Chen, C.-J. Chu, Journal of The Electrochemical Society 158/6 (2011) D395; https://doi.org/10.1149/1.3575161
[30]S.-B. Zhu, Y. Geng, H.-L. Lu, Y. Zhang, Q.-Q. Sun, S.-J. Ding, D.W. Zhang, Journal of Alloys and Compounds (2013).
[31]Y. Geng, Z.-Y. Xie, W. Yang, S.-S. Xu, Q.-Q. Sun, S.-J. Ding, H.-L. Lu, D.W. Zhang, Surface and Coatings Technology/0 (2013).
[32] M. Ahmad, Z. Iqbal, Z.L. Hong, J.X. Yang, Y.W. Zhang, N.R. Khalid, E. Ahmed, Integr Ferroelectr 145/1 (2013) 108; https://doi.org/10.1080/10584587.2013.788943
[33]H.-A. Chin, I.-C. Cheng, C.-I. Huang, Y.-R. Wu, W.-S. Lu, W.-L. Lee, J.Z. Chen, K.-C. Chiu, T.-S. Lin, Journal of Applied Physics 108/5 (2010) 054503; https://doi.org/10.1063/1.3475500
[34] S.-T. Lien, H.-C. Li, Y.-J. Yang, C.-C. Hsu, I.-C. Cheng, J.-Z. Chen, Journal of Physics D: Applied Physics 46/7 (2013) 075202; https://doi.org/10.1088/0022-3727/46/7/075202
[35] H.A. Chin, I.C. Cheng, C.K. Li, Y.R. Wu, J.Z. Chen, W.S. Lu, W.L. Lee, J Phys D Appl Phys 44/45 (2011) 455101; https://doi.org/10.1088/0022-3727/45/45/455101
[36] T.-H. Wu, J.-Z. Chen, C.-C. Hsu, I.-C. Cheng, Journal of Physics D: Applied Physics 47/25 (2014) 255102; https://doi.org/10.1088/0022-3727/47/25/255102
[37] W. Chen, W. Zhu, O. K. Tan, and X. F. Chen, J. Appl. Phys., 108, 034101 (2010); https://doi.org/10.1063/1.3457217
[38]Q. Xu, M. T. Lanagan, W. Luo, L. Zhang, J. Xie, H. Hao, M. Cao, Z. Yao, and H. Liu, J. Eur.Ceram. Soc., 36, 2469 (2016); https://doi.org/10.1016/j.jeurceramsoc.2016.03.011
[39]X. Zhou, Y.-a. Zhang, W. Shi, T. Guo, Journal of Materials Science: Materials in Electronics (2012) 1.
[40]X. Zhou, D. Jiang, F. Lin, X. Ma, W. Shi, Physica B: Condensed Matter 403/1 (2008) 115; https://doi.org/10.1016/j.physb.2007.08.087
[41]C.-H. Li, J.-Z. Chen, I. Cheng, Journal of Applied Physics 114/8 (2013) 084503; https://doi.org/10.1063/1.4819232
[42]C.-H. Li, J.-Z. Chen, Journal of Alloys and Compounds 601 (2014) 223; https://doi.org/10.1016/j.jallcom.2014.02.172
[43] C.H. Ahn, M.G. Yun, S.Y. Lee, H.K. Cho, IEEE Transactions on Electron Devices 61 (2014) 73; https://doi.org/10.1109/TED.2013.2288925
[44] W.S. Kim, S.Y. Shin, J.W. Park, Journal of the Electrochemical Society 159/4 (2012) H353; https://doi.org/10.1149/2.002204jes
[45]J.W. Park, W.S. Kim, Y.K. Moon, K.T. Kim, S.Y. Shin, B. Du Ahn, J.H. Lee, Electrochem Solid St 13/9 (2010) Ii295; https://doi.org/10.1149/1.3447862
[46]J. Biscaras, N. Bergeal, S. Hurand, C. Grossetête, A. Rastogi, R. Budhani, D. LeBoeuf,C. Proust, J. Lesueur, Physical review letters 108/24 (2012) 247004; https://doi.org/10.1103/PhysRevLett.108.247004
[47]A. Ohtomo, H. Hwang, Nature 427/6973 (2004) 423; https://doi.org/10.1038/nature02308
[48]A. Tsukazaki, S. Akasaka, K. Nakahara, Y. Ohno, H. Ohno, D. Maryenko, A. Ohtomo,M Kawasaki, Nat Mater 9/11 (2010) 889; https://doi.org/10.1038/nmat2874